Lasers in Medical Science (2019) 34:377–388
https://doi.org/10.1007/s10103-018-2608-4

ORIGINAL ARTICLE

Evaluation of theranostic perspective of gold-silica nanoshell for cancer nano-medicine: a numerical parametric study

Xiao Xu[1] · Yildiz Bayazitoglu[2] · Andrew Meade Jr[2]

Received: 21 May 2018 / Accepted: 2 August 2018 / Published online: 13 September 2018

Abstract

Using gold-silica nanoshell as a reference nano-agent, this work has performed preliminary numerical parametric study to investigate the feasibility and if feasible the efficiency of using a single nano-agent to achieve theranostic goals. In total, seven generics of gold-silica nanoshells have been tested including the $R[50, 10]$ (radius of the silica core is 50 nm and thickness of the gold shell is 10 nm), $R[40, 15]$, $R[55, 25]$, $R[40, 40]$, $R[75, 40]$, $R[104, 23]$, and $R[154, 24]$ nanoshells. A planar tissue model has been constructed as the platform for parametric study. For mathematical modeling, radiant transport equation (RTE) has been applied to describe the interactions among laser lights, the hosting tissue, and the hosted nanoshells and Penne's bio-heat equation has been applied to describe the hyperthermia induced by such interactions. Effects of different nanoshell generics on the diffuse reflectance signal and hyperthermia temperature transition have been simulated, basing on which the potential of a certain nanoshell generic as theranostic nano-agent has been evaluated. It has been found that it is highly feasible for gold-silica nanoshells to be engineered for theranostic purpose and nanoshell generics that are preferentially scattering should be explored for good theranostic candidates. On the condition that nanoshell generic with the right optical properties has been located, a moderate nanoshell retention in the target tissue site is already sufficient to induce effective theranostic effects, which indicates that theranostic nano-medicine might not have a stringent requirement for the delivery technique. Among nanoshells that have been tested, the $R[55, 25]$ nanoshell seems to be a promising candidate as theranostic nano-agent. Further testing on it is highly recommended. Nanoshells that are preferentially absorbing such as the $R[50, 10]$ and $R[40, 15]$ nanoshells are efficient photothermal agent and could be used for therapeutic purpose only. However, it is not recommended that preferentially absorbing nanoshells being used for theranostic purpose due to possible negative effects such nanoshells might bring to the diffuse reflectance signal.

Keywords Theranostic · Nano-medicine · Gold-silica nanoshell · Lasers · Cancer

Introduction

With nanoparticle-assisted therapeutics [1–6] and nanoparticle-assisted diagnostics [7–15], respectively moving from the bench to the clinic, theranostic nano-medicine is arising as a new research hot spot. Although the paradigm of theranostic nano-medicine has been in existence for barely a decade, many inspiring work and results have already been reported [16–27]. The word theranostic is coined from two words, therapeutic and diagnostic and it demonstrates the research ambition of constructing a nano-agent that is function-integrated and serves as a dual agent for both therapeutics and diagnostics. Various nano-structures could possibly be developed toward this goal including quantum dots, carbon nanotubes, nanostars, nanocages, nanospheres, nanopoporns, nanrods, and nanoshells. Expected applications of theranostic nano-agents include monitoring and quantifying the in vivo bio-distributions of nano-drugs [28–31] (e.g., recognizing nano-drug targeted accumulations, assessing longitudinal therapeutic efficacies), personalizing interventions between nano-drugs and other therapeutics, e.g., chemo-therapy [32–34] and above all, theranostic nano-medicine for cancer diagnosis and treatment [16, 17, 22, 23, 26, 27]. As

✉ Xiao Xu
xiao717@gmail.com

[1] Present address: Energy Research Institute, Shandong Academy of Science, Jinan, 250014, People's Republic of China

[2] Department of Mechanical Engineering, Rice University, Houston, TX, 77005, USA

an alarming fact, cancer is already the second top killer of human lives, surpassed only by heart diseases.

Although theranostic nano-medicine for cancers is still an emerging research topic, therapeutic nano-medicine for cancer treatments and diagnostic nano-medicine for cancer detections are in more mature stages. Previous studies have demonstrated that for diagnosis, scattering perspective of nanoparticles' plasmonic resonance should be exploited while for treatment, absorption perspective is the key focus. A big challenge for developing theranostic nano-medicine therefore is knowing how to locate a common ground, on which optical properties of a specific nano-agent are such that this nano-agent could work effectively to meet both therapeutic and diagnostic requirements. This work is a research step toward this challenge.

The gold shell, silica core (gold-silica) nanoshell, which is comprised with a silica core and a thin shell of gold, is used as reference nano-agent for this study. Compared to other nano-strucutres such as nanocage and nanosphere, gold-silica nanoshell is a more interest research object. Firstly, by controlling radius of the silica core, thickness of the gold shell and the ratio of shell thickness to silica core radius, optical characteristics of nanoshell are agilely tunable, which include (1) wavelength on which peak of the plasmonic resonance occurs, (2) optical orientation, i.e., whether the nanoshell generic is preferentially scattering or preferentially absorbing, and (3) absorption and scattering efficiencies of the nanoshell generic. Secondly, optical properties of gold-silica nanoshells could easily be tuned to be an order higher than those of nanocages and nanosphere [42, 49]. Research purpose of this study is to answer the following questions: (1) Is it feasible to achieve theranostic effects by using a single nanoshell generic? (2) If it is feasible, gold-silica nanoshells of what physical configurations and (consequently) optical properties would serve as good candidates for theranostic cancer nano-medicine?

This work is a numerical investigation, that is based on mathematical modeling and computational simulation. Although bench experiment remains to be the major tool for the development of cancer nano-medicine, it is also well recognized that numerical study could be a feasible alternative as well. Compared to bench-based experiments, computer-based simulations have unique advantages such as shorter research cycles, less monetary cost, easier to be set up for different tests, and cheaper to reproduce data. Bench study and numerical investigation work together could effectively accelerate the whole research progress: Data achieved by bench experiments provide essential information to set up reliable and realistic numerical simulations while data generated by simulations provide a preview of possible outcomes of certain experimental conditions and setups according to which the plan and design of experiments could be adjusted for an optimal production run. With modern high-performance computing (HPC) techniques, computation programs could even real-time monitor or guide experiment procedures. For researches on therapeutic nano-medicine and diagnostic nano-medicine, respectively, the helpful role of numerical investigation has already been well recognized and acknowledged [35–49]. Nevertheless, to the authors' best information, numerical investigation of function-integrated theranostic nano-medicine has never been reported yet. With such a background, this work is also an effort that aims at filling this void.

The rest of this paper is organized in the following order: In "Mathematical modeling", mathematical modeling of theranostic perspectives of gold-silica nanoshells would be introduced with detailed governing equations and boundary conditions being presented. In "Implementation verification", implementation of method presented in "Mathematical modeling" would be verified by several classical reference problems. In "Results and discussions", by means of constructing parametric study cases, several generics of gold-silica nanoshells with different optical properties would be analyzed as candidates for theranostic nano-agent. Discussions would be organized around results of the parametric study cases. In "Conclusions", major findings of this work would be summarized.

Mathematical modeling

The fundamentals of cancer nano-medicine are interactions among laser lights, the hosting biological tissues, and the hosted nanoparticles (gold-silica nanoshells in this work). All partially or fully controllable factors such as nanoshell generic, delivery and accumulation of nanoshell at the target site, wavelength of source laser, dosage of laser power, and exposure time of laser irradiance are arranged in such a way that depending on the specific medical goal, distribution of either optical signals, or fluence rate, or bio-heat generation, or the induced hyperthermia temperature could be as desirable as possible. As the external irradiance, lasers from the near-infrared (NIR) spectrum are preferred since most biology tissues are low absorbent to lights from this spectrum, allowing them to penetrate deep without being extinct. The NIR spectrum is recognized as the optical gateway for medicine.

Governing equations and boundary conditions

The radiant transport equation (RTE) [51–53] could be applied to describe interactions among laser lights, the hosting biological tissues and the hosted nanoparticles. The

temporal, integral-differential form RTE is the deterministic equivalence of Monte Carlo ray tracing and could be written as:

$$\frac{1}{c}\frac{\partial L(\boldsymbol{r},\boldsymbol{s})}{\partial t}+\frac{\partial L(\boldsymbol{r},\boldsymbol{s})}{\partial \boldsymbol{s}}+(k_\alpha(\boldsymbol{r})+k_s(\boldsymbol{r}))L(\boldsymbol{r},\boldsymbol{s}) = \frac{k_s(\boldsymbol{r})}{4\pi}\int_{4\pi}\Phi(\boldsymbol{s},\boldsymbol{s}')L(\boldsymbol{r},\boldsymbol{s}')d\Omega' \quad (1)$$

where $\boldsymbol{r}$ and $\boldsymbol{s}$ indicate the position and direction vectors respectively, $L(\boldsymbol{r},\boldsymbol{s})$ indicates the local, directional radiant intensity, $k_s(\boldsymbol{r})$ and $k_\alpha(\boldsymbol{r})$ indicate local scattering and absorption coefficients respectively, Ω indicates the solid angle, $\Phi(\boldsymbol{s},\boldsymbol{s}')$ indicates the phase function between directions $\boldsymbol{s}$ and $\boldsymbol{s}'$, c indicates the velocity with which the laser light travels within the tissue medium, and t indicates the time. This study adopts a continuous wave (CW) laser, temporal term $\frac{1}{c}\frac{\partial L(\boldsymbol{r},\boldsymbol{s})}{\partial t}$ in Eq. 1 therefore is simply neglected.

For non-emitting, diffusively reflective boundaries, the associated boundary condition could be written as:

$$L(\boldsymbol{r},\boldsymbol{s}) = q_0\delta(\boldsymbol{s}-\boldsymbol{s_c})+\frac{\rho}{\pi}\int_{\boldsymbol{n}\cdot\boldsymbol{s}'<0}L(\boldsymbol{r},\boldsymbol{s}')|\boldsymbol{n}\cdot\boldsymbol{s}'|d\Omega' \quad (2)$$

where q_0 indicates magnitude of the laser irradiance, $\boldsymbol{s}_c$ indicates propagating direction of the collimated laser lights, $\boldsymbol{n}$ indicates normal vector of a specific boundary position, δ indicates the Dirac delta function, and ρ indicates the diffuse reflection coefficient.

Before nanoshells being deposited to the biological tissue, $k_\alpha(\boldsymbol{r})$ and $k_s(\boldsymbol{r})$ in Eq. 1 are local absorption and scattering coefficients of the hosting tissue and Eq. 1 mathematically describes interactions between laser lights and the tissue medium within which the lights are traveling through. After nanoshells being deposited to the tissue, $k_\alpha(\boldsymbol{r})$ and $k_s(\boldsymbol{r})$ are overall absorption and scattering coefficients that take both tissue and nanoshells into account:

$$\begin{aligned} k_\alpha(\boldsymbol{r}) &= k_{\alpha,t}(\boldsymbol{r})+k_{\alpha,ns}(\boldsymbol{r}) \\ k_s(\boldsymbol{r}) &= k_{s,t}(\boldsymbol{r})+k_{s,ns}(\boldsymbol{r}) \end{aligned} \quad (3)$$

where subscripts "t" and "ns" identify the tissue and nanoshells, respectively. Equation 1 now describes interactions among laser lights, the hosting biology tissues, and the hosted nanoshells. Note that $k_{\alpha,ns}(\boldsymbol{r})$ and $k_{s,ns}(\boldsymbol{r})$ could be quantified by absorption and scattering efficiencies $Q_{\alpha,ns}$ and $Q_{s,ns}$ [35–41, 43–45] as:

$$\begin{aligned} k_{\alpha,ns} &= C_\alpha N_T = \pi r_0^2 Q_{\alpha,ns} N_T \\ k_{s,ns} &= C_s N_T = \pi r_0^2 Q_{s,ns} N_T \end{aligned} \quad (4)$$

where C_α and C_s indicate absorption and scattering cross sections of a nanoshell generic, N_T indicates the nanoshell density(i.e., the number of nanoshell particles per unit volume) and r_0 indicates radius of the silica core of a single nanoshell particle. The Mie theory [62] could be applied to approximate $Q_{\alpha,ns}$ and $Q_{s,ns}$. In total seven generics of gold-silica nanoshells would be studied in this work including the $R[50, 10]$ (radius of the silica core is 50 nm and thickness of the gold shell is 10 nm), $R[40, 15]$, $R[55, 25]$, $R[40, 40]$, $R[75, 40]$, $R[104, 23]$ and $R[154, 24]$ nanoshells.

For turbid medium such as biology tissues, the Henyey-Greenstein phase function [61] is an appropriate representation of $\Phi(\boldsymbol{s}',\boldsymbol{s})$ in Eq. 1:

$$\Phi(\boldsymbol{s}',\boldsymbol{s}) = \frac{1}{4\pi}\frac{1-g^2}{[1+g^2-2g\cos(\boldsymbol{s}\cdot\boldsymbol{s}')]^{1.5}} \quad (5)$$

Where g indicates the anisotropy factor, which is in the range of [-1, 1]. Note $g = 0$ indicates an isotropic scattering, $g > 0$ indicates a preferentially forward scattering, and $g < 0$ indicates a preferentially backward scattering. For biology tissues, g typically is in the range of [0.7, 1) [51].

Radiant intensity $L(\boldsymbol{r},\boldsymbol{s})$ in Eq. 1 is comprised with two parts, i.e., the remnant of laser irradiance $L_c(\boldsymbol{r},\boldsymbol{s})$ and the induced diffusion radiation $L_d(\boldsymbol{r},\boldsymbol{s})$:

$$L(\boldsymbol{r},\boldsymbol{s}) = L_d(\boldsymbol{r},\boldsymbol{s})+L_c(\boldsymbol{r},\boldsymbol{s}) \quad (6)$$

According to the Beer-Lambert law [51], magnitude of laser irradiance q_0 decays exponentially as the light travels in the tissue medium:

$$L_c(\boldsymbol{r},\boldsymbol{s}) = q_0\exp(-(k_\alpha(\boldsymbol{r})+k_s(\boldsymbol{r}))(\boldsymbol{r}-\boldsymbol{r}_b))\delta(\boldsymbol{s}-\boldsymbol{s_c}) \quad (7)$$

where $\boldsymbol{r}-\boldsymbol{r}_b$ indicates absolute distance the light has traveled after its entrance from the boundary position $\boldsymbol{r}_b$.

Substitute Eqs. 6 and 7 back to Eq. 1, governing equation for $L_d(\mathbf{r},\mathbf{s})$ is derived as:

$$\frac{\partial L_d(\boldsymbol{r},\boldsymbol{s})}{\partial \boldsymbol{s}}+(k_\alpha(\boldsymbol{r})+k_s(\boldsymbol{r}))L_d(\boldsymbol{r},\boldsymbol{s}) = \frac{k_s(\boldsymbol{r})}{4\pi}\int_{4\pi}\Phi(\boldsymbol{s},\boldsymbol{s}')L_d(\boldsymbol{r},\boldsymbol{s}')d\Omega'+\frac{k_s(\boldsymbol{r})}{4\pi}\Phi(\boldsymbol{s},\boldsymbol{s_c})L_c(\boldsymbol{r},\boldsymbol{s}) \quad (8)$$

Correspondingly, boundary condition for $L_d(\mathbf{r},\mathbf{s})$ could be derived from Eq. 2 as:

$$L_d(\boldsymbol{r},\boldsymbol{s}) = \frac{\rho}{\pi}\int_{\boldsymbol{n}\cdot\boldsymbol{s}'<0}L_d(\boldsymbol{r},\boldsymbol{s}')\left|\boldsymbol{n}\cdot\boldsymbol{s}'\right|d\Omega' \quad (9)$$

Equations 8–9 requires a numerical approximation, for which methods such as discrete ordinate (DO) [56–58] and finite volume (FV) [37–39, 58–60] are both well established alternatives. This work adopts the latter one.

Nanoshell-assisted diagnostics

The most important diagnostic application for gold-silica nanoshell is being used as exogenous optical contrast agent for the optical imaging technique including optical confocal microscopy (OCM) [63], optical coherence tomography

(OCT) [64], diffuse reflectance spectroscopy [65] and diffuse optical tomography (DOT). The optical imaging technique enables detective laser lights to penetrate into tissues as deep as several hundred micro-meters and non-invasively capture images with a resolution of micro-meters, which is 1 to 2 orders finer than what the more conventional magnetic resonance imaging (MRI) could achieve [42, 65]. This technique has shed new hopes to early-stage cancer detections, which are notoriously difficult since disease signatures are usually too subtle to be captured by conventional imaging modalities such as MRI. For the purpose of diagnosis, hemispherical diffuse reflectance is the most important optical signal. To evaluate the feasibility and (if feasible) the efficiency of a specific gold-silica nanoshell generic as the exogenous optical contrast agent, its capability of affecting the diffuse reflection signal should be assessed.

Nanoshell-assisted therapeutics

The most important therapeutic application for gold-silica nanoshell is being used as exogenous photothermal agent for the photothermal therapy (PTT), which fundamentally is a heat-based treatment plan that intends to burn out the target cancerous tissue. For conventional PTT, while the target cancerous tissues being destructed by the laser exposure, healthy tissues that surround the cancerous tissue are likely to be seriously damaged as well. This is referred as the "invasive" or "non-selective" problem of this therapy, which has seriously limited its application.

When nanoshells are used as exogenous photothermal agent, these particles are embedded to the cancerous tissue only. The surrounding healthy tissues are kept clean of them. The embedded nanoshells are engineered to be such that they are efficient photon absorbers. Once exposed to laser irradiance, these particles point-wisely convert laser photon energy to bio-heat and dissipate the heat out to their surrounding tissue environment within picoseconds [66]. It is expected that such enhanced energy conversion and bio-heat generation in the cancerous tissue could enable the threshold laser dosage for the cancerous tissues destruction to such a level that it is safe for the surrounding healthy tissue. The "non-selective" problem of the conventional PTT is therefore bypassed.

During laser exposure, local intensity of photon energy could be quantified by fluence rate $G(\boldsymbol{r})$:

$$G(\boldsymbol{r}) = \int_{4\pi} (L_c(\boldsymbol{r}, \boldsymbol{s}) + L_d(\boldsymbol{r}, \boldsymbol{s}))d\Omega \tag{10}$$

The conversion from laser photon energy to bio-heat could be quantified as:

$$q(\boldsymbol{r}) = k_\alpha(\boldsymbol{r})G(\boldsymbol{r}) = (k_{\alpha,t}(\boldsymbol{r}) + k_{\alpha,ns}(\boldsymbol{r})) \int_{4\pi} (L_c(\boldsymbol{r}, \boldsymbol{s}) + L_d(\boldsymbol{r}, \boldsymbol{s}))d\Omega \tag{11}$$

Note that $q(\boldsymbol{r})$ is also recognized as the local heat source, which inevitably would change temperature field within the tissue. Penne's bio-heat equation [37, 38, 66] could be used to describe such change, which under the Cartesian coordinate system is of the following form:

$$\rho c_p \frac{\partial T}{\partial t} = \frac{\partial}{\partial x}\left(K\frac{\partial T}{\partial x}\right) + \frac{\partial}{\partial y}\left(K\frac{\partial T}{\partial y}\right) - v_B(T - T_{Arterial}) + q_r \tag{12}$$

where T indicates the local temperature, $T_{Arterial}$ indicates temperature at the arterials, ρ, c_p and K indicates the density, specific heat, and thermal conductivity of the tissue medium, respectively and v_B indicates the blood perfusion rate. If the tissue slab is cooled by nature convection, the boundary condition could simply be expressed as:

$$K\frac{\partial T}{\partial y}|_{x,y} = h(T - T_\infty) \tag{13}$$

where h is the convection coefficient and T_∞ is the environment temperature.

To evaluate the feasibility and (if feasible) the efficiency of nanoshells as the exogenous photothermal agent, their capability of affecting the temperature field and inducing the hyperthermia should be assessed.

Implementation verification

As "Mathematical modeling" has demonstrated, RTE solution is the key of the whole simulation, which not only takes up the majority of simulation time but also determines the reliability of the simulation. An FV-based RTE solver has been developed in-house. To validate the solver, it has been applied to simulate several classic reference problems.

Geometry for all the reference problems is a two-dimensional (2-D) square shaped domain enclosed by cold ($T = 0$ K) black walls. Length of the domain is 1 m. Emitting-absorbing-scattering gaseous medium is enclosed in the domain, temperature of which is kept such that $\sigma T^4/\pi = 1\ W/m^2$ (σ is the Stefan-Boltzman constant). The extinction coefficient $\beta = k_\alpha + k_s$ and the scattering albedo $\omega = \frac{k_s}{\beta}$ of the gaseous medium have been varied to construct six different cases: (1) case 1: $\beta = 10.0\ m^{-1}$ and $\omega = 0.0$, (2) case 2: $\beta = 4.0\ m^{-1}$ and $\omega = 0.0$, (3) case 3: $\beta = 1.0\ m^{-1}$ and $\omega = 0.0$, (4) case 4: $\beta = 0.25\ m^{-1}$ and $\omega = 0.0$, (5) case 5: $\beta = 1.0\ m^{-1}$, $\omega = 0.5$ and the scattering is isotropic, (6) case 6: $\beta = 1.0\ m^{-1}$, $\omega = 0.9$ and the scattering is isotropic. Non-dimensional heat flux at the bottom boundary has been computed for all the cases and the results are compared against published data contributed by Howell et al [67], which were generated by the zone

method. The comparison is presented as Fig. 1 with Fig. 1a presenting results of cases 1, 2, and 3 and Fig. 1b presenting results of cases 4, 5, and 6. Symbols in the figure correspond to results from the reference while lines corresponds to results of our own implementation. It could be seen that agreement between the two implementations is very good, confirming the reliability of our implementation.

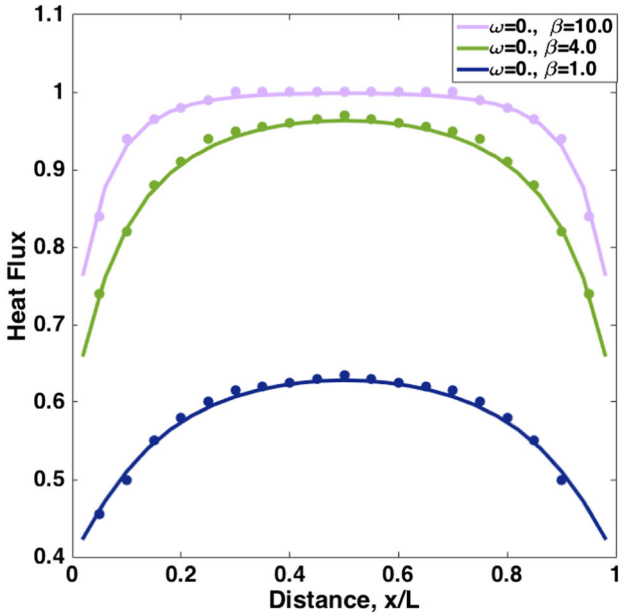

(a) Case 1, 2 and 3: the emitting-absorbing gray gas

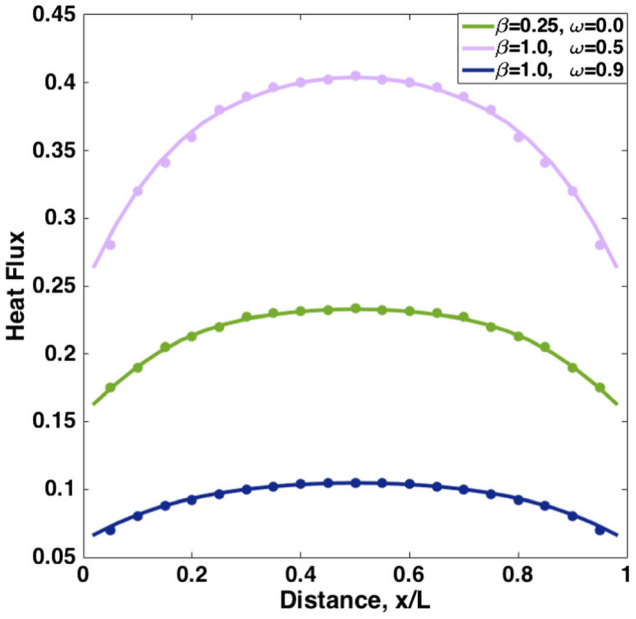

(b) Case 4, 5 and 6: the emitting-absorbing-scattering gray gas

Fig. 1 Non-dimensional heat flux along the bottom boundary for cases 1–6

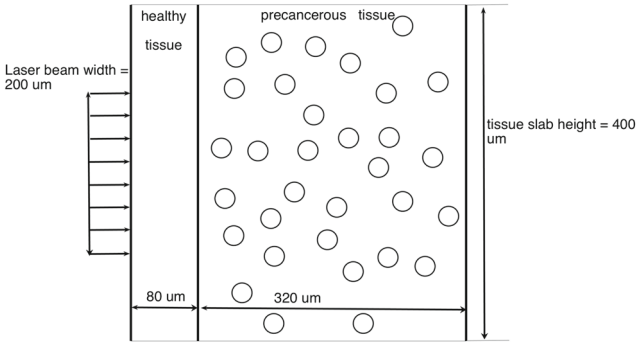

Fig. 2 Illustration of the planar tissue model

Results and discussions

In this section, the achievability of theranostic effects by using a single nanoshell generic would be investigated. A planar tissue model as Fig. 2 illustrates has been constructed, according to which, a collimated laser beam irradiates a tissue slab from the left. Wavelength of the beam is 830 nm and width of which is 100 µm. The tissue slab is comprised with both healthy and cancerous tissues. The healthy tissue is exposed directly to laser irradiance while the cancerous tissue hides behind. The healthy tissue is of a thickness of 80 µm and the cancerous tissue is of a thickness of 320 µm. Height of the tissue slab is 400 µm, which is the same as its thickness.

The references [54, 55] present optical properties of biology tissues under different infrared (IR) and NIR wavelengths, basing on which this work sets optical properties of healthy and cancerous tissues for the wavelength of 830 nm to be: $k_\alpha = 0.4\ \text{mm}^{-1}$, $k_s = 10\ \text{mm}^{-1}$, and $g = 0.92$ for healthy tissue while $k_\alpha = 0.15\ \text{mm}^{-1}$, $k_s = 10\ \text{mm}^{-1}$, and $g = 0.92$ for cancerous tissue. Table 1 tabulates $Q_{s,ns}$, $Q_{\alpha,ns}$, and g for the wavelength of 830 nm for different nanoshell generics, including the $R[50, 10]$, $R[40, 15]$, $R[55, 25]$, $R[40, 40]$, $R[75, 40]$, $R[104, 23]$, and $R[154, 24]$ nanoshells. The original data has been published by Lin [49].

Necessary condition for any nano-medicine to be effective is that a sufficient dosage could be delivered to the target site. For example, McCarthy et al. [50] have reported that for their nanoparticle-assisted imaging trails, the threshold nanoparticle dosage is 0.5–1.0 µg/kg boy weight and if nanoparticle accumulation in the target tissue site is lower than this value, nanoparticles only have trivial impacts on the trail results. Delivery and accumulation of nano-medicine to a target site is a complicated process and itself is an research hot spot. Many factors could affect nano-medicine accumulation including the drug delivery technique, drug release, and accumulation mechanism, and organ clearance mechanism.

Table 1 Optical properties of different nanoshell generics for the wavelength of 830 nm

Nanoshell	ω	$Q_{s,ns}$	$Q_{\alpha,ns}$	$C_s(\text{mm}^2)$	$C_\alpha(\text{mm}^2)$	g	$N_T(\frac{1}{\text{mm}^3})$	$k_{s,ns}(\frac{1}{\text{mm}})$	$k_{\alpha,ns}(\frac{1}{\text{mm}})$
$R[50, 10]$	0.2748	1.11	2.93	8.7135E-9	2.3000E-8	N/A	7.014E7	0.611	1.613
$R[40, 15]$	0.4118	1.08	1.54	5.4259E-9	7.7370E-9	N/A	9.105E7	0.494	0.705
$R[55, 25]$	0.7613	3.38	1.06	3.2105E-8	1.0068E-8	N/A	2.960E7	0.949	0.298
$R[40, 40]$	0.8634	3.22	0.51	1.6177E-8	2.5622E-9	N/A	2.960E7	0.478	0.076
$R[75, 40]$	0.9001	3.33	0.37	5.8816E-8	6.5351E-9	N/A	9.954E6	0.585	0.065
$R[104, 23]$	0.7692	2.83	0.85	9.6113E-8	2.8868E-8	0.148	7.396E6	0.711	0.213
$R[154, 24]$	0.7574	3.09	0.99	2.3011E-7	7.3724E-8	0.457	2.685E6	0.618	0.198

This work uses volume fraction V_f to quantify nanoshell accumulation within the target site, which is defined as:

$$V_f = \frac{\text{volume of nanoshells}}{\text{volume of tissue slab}} \times 100 \tag{14}$$

Note that "volume of nanoshells" in Eq. 14 is determined by both the in total number of embedded nanoshells and the volume of a single nanoshell particle. Following the discussion of Lin [42, 49] on the feasible range of nanoshell retentate, this work sets V_f to be 0.00675. Correspondingly, N_T for each nanoshell generic has been calculated and the results are listed in Table 1. Note that for the same V_f, N_T is different for differet nanoshell generics since the volume of a single nanoshell particle is different. After N_T is decided, $k_{\alpha,ns}$ and $k_{s,ns}$ for each nanoshell generic could be computed following Eq. 4. The calculated results are presented in Table 1 as well.

Diagnostic effects of nanoshells

To evaluate diagnostic perspectives of nanoshells, their capability of affecting the diffuse reflectance signal needs to be investigated.

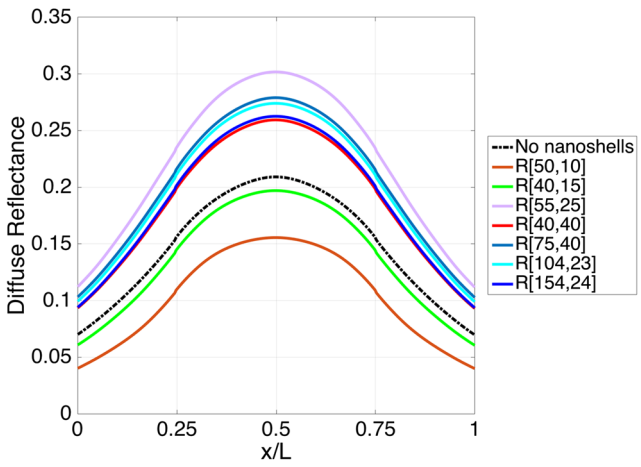

Fig. 3 The distribution of diffuse reflectance along the left boundary of the tissue slab, without and with nanoshells embedded in the cancerous tissue as exogenous optical contrast agent

The distribution of diffuse reflectance along left boundary of the tissue slab has been computed and the results are presented as Fig. 3. The $x-$ axis of Fig. 3 corresponds to the normalized position x/H with H being the height of tissue slab. The $y-$ axis corresponds to the normalized diffuse reflectance. The normalization is against q_0, magnitude of the collimated radiant intensity. The black dash-dot line in the figure corresponds to the distribution of diffuse reflectance signal when no nanoshells of any generics have been embedded in the cancerous tissue. Solid lines of different colors correspond to the distributions of diffuse reflectance signal when different nanoshell generics have been embedded.

It is seen clearly from Fig. 3 that nanoshells embedded in the cancerous tissue site do affect the diffuse reflectance. Specifically, the $R[55, 25]$, $R[40, 40]$, $R[75, 40]$, $R[104, 23]$, and $R[154, 24]$ nanoshells all enhance the diffuse reflectance signal with the $R[55, 25]$ nanoshell enhancing the signal the most. On the other hand, the $R[50, 10]$ and $R[40, 15]$ nanoshells diminish the diffuse reflectance signal.

To better quantify alterations in the diffuse reflectance brought by nanoshells, Table 2 tabulates peaks of the diffuse reflectance (see the "Peak" column), with and without nanoshells embedded in the cancerous tissue. Differences in the diffuse reflectance peak (see the "Diff(%)" column)

Table 2 The peak of diffuse reflectance, without and with nanoshells embedded in the cancerous tissue as the exogenous optical contrast agent

	Peak	Diff(%)
No nanoshells	0.209	
$R[50, 10]$	0.156	−25.4
$R[40, 15]$	0.197	−5.7
$R[55, 25]$	0.302	44.5
$R[40, 40]$	0.259	23.9
$R[75, 40]$	0.279	33.5
$R[104, 23]$	0.274	31.1
$R[154, 24]$	0.263	25.8

(Diff(%): difference in the peak of diffuse reflectance induced by nanoshells)

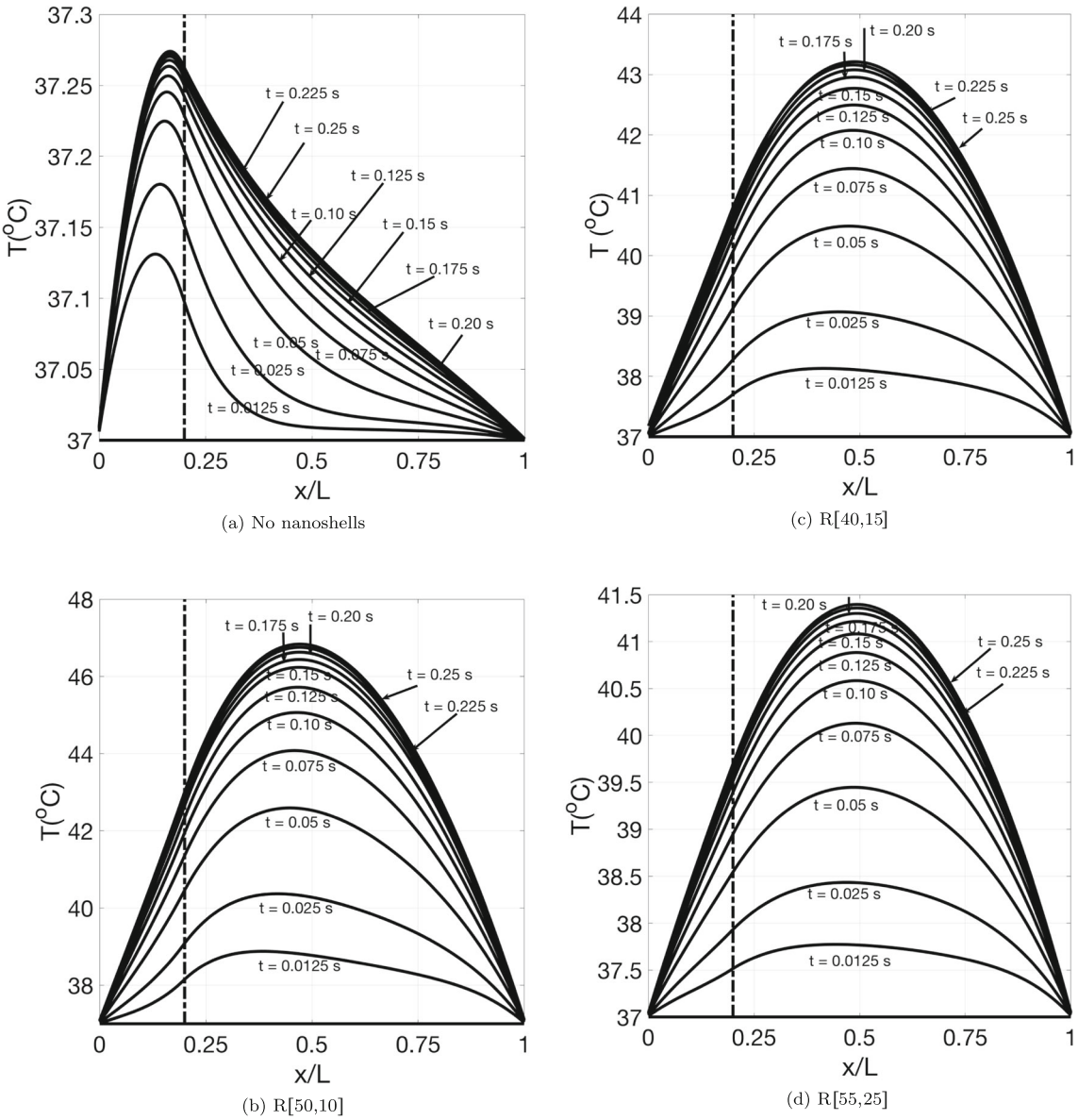

(a) No nanoshells

(c) R[40,15]

(b) R[50,10]

(d) R[55,25]

Fig. 4 Temperature transition on the half-plane of the tissue slab with different nanoshell generics embedded in the cancerous tissue site as the exogenous photothermal agent: **a** No nanoshells, **b** the R[50,10] nanoshell, **c** the R[40,15] nanoshell, **d** the R[55,25] nanoshell, **e** the R[40,40] nanoshell, **f** the R[75, 40] nanoshell, **g** the R[104, 23] nanoshell, and **h** the R[154, 24] nanoshell

induced by nanoshells are computed and presented in the same table as well. It is seen that before the addition of any nanoshells, the diffuse reflectance peak is 0.209. The $R[55, 25]$, $R[40, 40]$, $R[75, 40]$, $R[104, 23]$, and $R[154, 24]$ nanoshells, respectively promote this value to 0.302 (an increment of +44.5%), 0.259 (+23.9%), 0.279 (+33.5%), 0.274 (+31.1%), and 0.263 (+25.8%). On the other hand, the $R[50, 10]$ and $R[40, 15]$ nanoshells bring down the original diffuse reflectance peak of 0.209 to 0.156 (a decrement of − 25.4%) and 0.197 (− 5.7%), respectively.

Figure 3 and Table 2 together demonstrate that a small dosage of nanoshells (e.g., nanoshell volume fraction $V_f = 0.00675$) is already sufficient to alter the diffuse reflectance appreciably. From the diagnostic perspective, the $R[55, 25]$, $R[75, 40]$, and $R[104, 23]$ nanoshells all seem to be good candidates for exogenous optical contrast agent because of their capability of enhancing the diffuse reflectance signal. It is also noticed that the preferentially absorbing $R[50, 10]$ and $R[40, 15]$ nanoshells should be avoided being used for diagnostic purposes.

Therapeutic effects of nanoshells

Further, therapeutic perspectives of different nanoshell generics are investigated. According to [72], for both healthy and cancerous tissues, tissue density ρ is set to

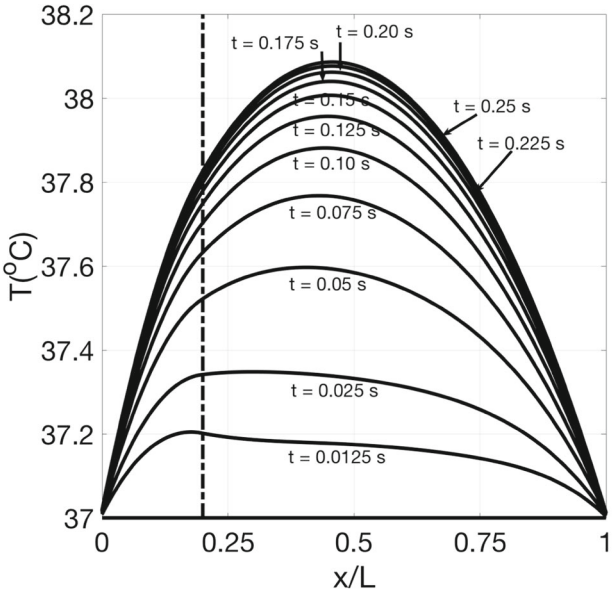

(e) R[40,40]

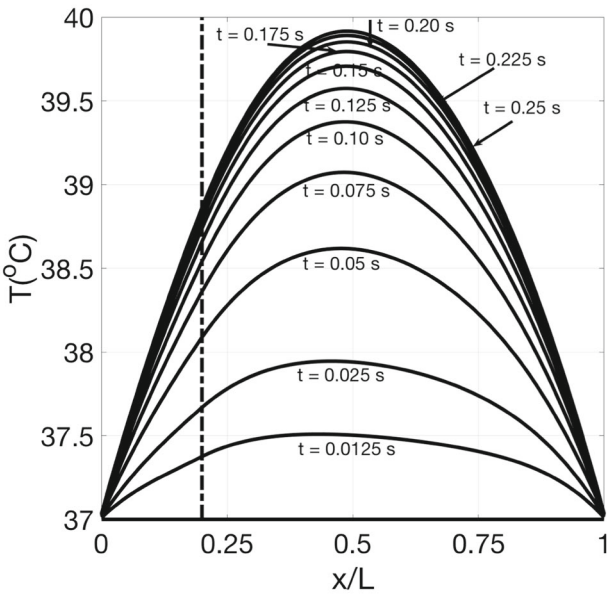

(g) R[104,23]

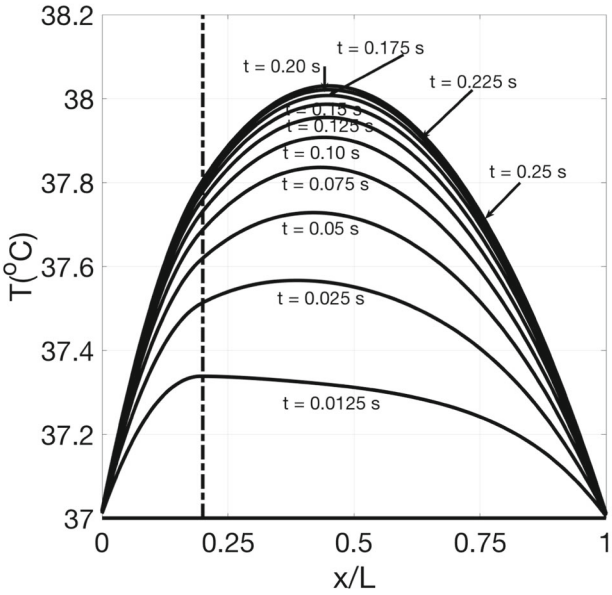

(f) R[75,40]

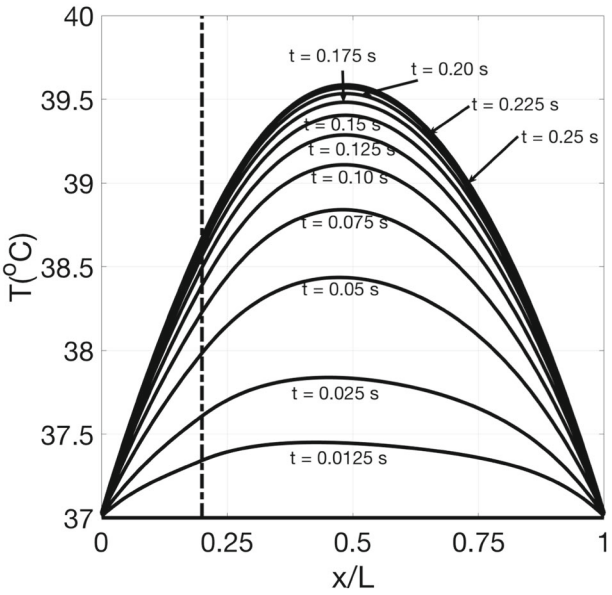

(h) R[154,24]

Fig. 4 (continued)

be 1090 kg/m^3 and heat conductivity K is set to be 0.45 W/m K. Specific heat c_p is 3400 J/kg $\cdot$ K for the cancerous tissue and 3370 J/kg $\cdot$ K for the healthy tissue. Therapeutic perspectives of nanoshells are mainly judged by the particles' capability of inducing hyperthermia, for which temperature is the key parameter. Initially, the whole tissue slab is assumed to be of 37 $^\circ C$. The Dirichlet boundary condition is implemented for all boundary surfaces and the temperature is fixed to be 37 $^\circ C$.

Figure 4 presents temporal transition of temperature field on the half-plane of the tissue slab with Fig. 4a corresponding to the situation that no nanoshells of any generics have been embedded in the cancerous tissue while Fig. 4b–g, respectively corresponding to situations that the R[50, 10], R[40, 15], R[55, 25], R[40, 40], R[75, 40], R[104, 23], and R[154, 24] nanoshells have been embedded in the cancerous tissue. The $x-$axis corresponds to the normalized depth x/L with L being thickness of the tissue

slab. The $y-$axis corresponds to the temperature (unit $^{\circ}C$). The dashed-dot line that is vertical to the $x-$axis identifies the differentiation line between healthy and cancerous tissues (see Fig. 2).

Since temperatures for all boundary faces are fixed to be 37 $^{\circ}C$, temperature field within the tissue slab eventually would reach the steady state. Figure 4a shows that without any nanoshells being embedded in the cancerous tissue, temperature peak on the half-plane occurs in the healthy tissue site. Besides, average temperature in the healthy tissue site is significant higher than that in the cancerous tissue site, which implies that the healthy tissue would be damaged before the cancerous tissues. Such effect is most undesirable for therapeutic purposes. Figure 4b–g demonstrate that after nanoshells being embedded in the cancerous tissue, no matter the nanoshells are preferentially absorbing or preferentially scattering, temperature peak of the half-plane starts to transit from the healthy tissue site to the cancerous tissue site. Besides, average temperature in the cancerous tissue site rises to be higher than that in the healthy tissue site, which is despite of the fact that the healthy tissue is directly exposed to the laser irradiance while the cancerous tissue is hiding behind it. Such effects are desirable for therapeutic purposes.

To assess therapeutic perspectives of different nanoshell generics more quantitatively, Table 3 presents peak of the steady state temperature field (see T_{max} column), without and with nanoshells embedded in the cancerous tissue. It is seen that without nanoshells, temperature peak occurs in the healthy tissue site and is of the value of 37.27 $^{\circ}C$, which is only 0.27 $^{\circ}C$ higher than the initial temperature of 37 $^{\circ}C$. After the $R[50, 10]$, $R[40, 15]$, $R[55, 25]$, $R[40, 40]$, $R[75, 40]$, $R[104, 23]$, and $R[154, 24]$ nanoshells, respectively being embedded in the cancerous tissue, temperature peak occurs in the cancerous tissue site and increases to 46.83 $^{\circ}C$ (an increment of 9.83 $^{\circ}C$), 43.21 $^{\circ}C$ (6.21 $^{\circ}C$), 41.40 $^{\circ}C$ (4.40 $^{\circ}C$), 38.09 $^{\circ}C$ (1.09 $^{\circ}C$), 38.03 $^{\circ}C$ (1.03 $^{\circ}C$), 39.92 $^{\circ}C$ (2.92 $^{\circ}C$), and 39.59 $^{\circ}C$ (2.50 $^{\circ}C$), respectively from the initial temperate of 37 $^{\circ}C$. Judged by the induced hyperthermia, the preferentially absorbing $R[50, 10]$ and $R[40, 15]$ nanoshells are the best photothermal agent. However, nanoshells that are preferentially scattering could be engineered to be sufficiently efficient photothermal agent as well. The $R[55, 25]$, $R[104, 23]$, and $R[154, 24]$ nanoshells all haven shown good potentials, among which the $R[55, 25]$ nanoshell is the most promising one.

Table 3 Temperature peak (T_{max}) on the half-plane without and with different nanoshell generics embedded in the cancerous tissue as exogenous photothermal agent

	T_{max}	ΔT
No nanoshells	37.27	0.27
$R[50, 10]$	46.83	9.83
$R[40, 15]$	43.21	6.21
$R[55, 25]$	41.40	4.40
$R[40, 40]$	38.09	1.09
$R[75, 40]$	38.03	1.03
$R[104, 23]$	39.92	2.92
$R[154, 24]$	39.59	2.50

(ΔT: difference in T_{max} due to nanoshells)

Theranostic effects of nanoshells

To be used as theranostic agent, the specific nanoshell generic needs to be effective and efficient for both diagnostic and therapeutic purposes. In "Diagnostic effects of nanoshells", it has been demonstrated that the $R[55, 25]$, $R[40, 40]$, $R[75, 40]$, $R[104, 23]$, and $R[154, 24]$ nanoshells all work effectively as exogenous optical contrast agent, enhancing the diffuse reflectance signal significantly. If rank these five nanoshell generics according to their capacity of promoting the diffuse reflectance signal, the order should be $R[55, 25]$, $R[75, 40]$, $R[104, 23]$, $R[154, 24]$, and $R[40, 40]$ with the $R[55, 25]$ nanoshell enhancing the diffuse reflectance the most. In "Therapeutic effects of nanoshells", it has been demonstrated that besides the preferentially absorbing $R[50, 10]$ and $R[40, 15]$ nanoshells, the preferentially scattering $R[55, 25]$, $R[104, 23]$, and $R[154, 24]$ nanoshells also work effectively and efficiently as photothermal agent with the $R[55, 25]$ nanoshell showing the best potentials of the three. Judged from both the therapeutic and diagnostic perspectives, the $R[55, 25]$ nanoshell seems to be the best candidate as theranostic nano-agent. Another advantage of the $R[55, 25]$ nanoshell is that overall size of a single particle of this nanoshell generic is small (radius of a single particle is only 80 nm), which enables more efficient nanoshell delivery and accumulation to the target cancerous tissue site. Previous researches [68–71] have demonstrated that the most fundamental mechanism for nanoshells to leak from blood circulation to the target tissue site is the enhanced permeability and retention effect (ERP). The smaller the nanoshell particle is, the easier it is for the particle to reach and accumulate in the target site.

Conclusions

This work has performed numerical parametric study to investigate the feasibility and if feasible the efficiency of gold-silica nanoshell as the theranostic nano-agent for both

cancer diagnosis and treatment. Seven nanoshell generics have been tested for such purpose including the $R[50, 10]$, $R[40, 15]$, $R[55, 25]$, $R[40, 40]$, $R[75, 40]$, $R[104, 23]$, and $R[154, 24]$ nanoshells. It has been found that nanoshell generics that are preferentially absorbing, e.g., the $R[50, 10]$ and $R[40, 15]$ nanoshells, might not be good candidates as the theranotic agent since such nanoshells are likely to diminish the diffuse reflection signal. Nevertheless, such nanoshells be engineered to be very good photothermal agent for therapeutic usage only. Nanoshells that are preferentially scattering should be tested to search for good candidates for theranostic agent. Among the five preferentially scattering nanoshells that have been tested, the $R[55, 25]$ nanoshell seems to be very promising and is worth further research. If nanoshell with the right optical properties has been located, accumulation rate of which in the target tissue site doesn't need to be very high to induce the desired theranostic effects, which implies that theranostic nano-medicine might not have a stringent requirement for the delivery technique.

Compliance with ethical standards

The authors certify that we Do Not have any affiliations with or involvement in any organization or entity with any financial interest or non-financial interest in the subject matter or materials discussed in this manuscript. NO human or animal participants have been involved for work presented in this manuscript.

References

1. Hirsch LR, Stafford RJ, Bankson JA, Sershen SR, Rivera B, Price RE, Hazle JD, Halas NJ, West JL (2003) Nanoshell-mediated near-infrared thermal therapy of tumors under magnetic resonance guidance. Proc Nat Acad Sci 100(23):13549–13554
2. O'Neal DP, Hirsch LR, Halas NJ (2004) Photo-thermal tumor ablation in mice using near infrared-absorbing nanoparticles. Cancer Lett 209(2):171–176
3. Goodrich G, Bao L, Gill-Sharp K, Sang K, Wang L, Payne J (2010) Photothermal therapy in a murine colon cancer model using near-infrared absorbing gold nanorods. J Biomed Opt 15(1):1–7
4. Lu W, Xiong C, Zhang G, Huang Q, Zhang R, Zhang J, Li C (2009) Targeted photothermal ablation of murine melanomas with melanocyte-stimulating hormone analog conjugated hollow gold nanospheres. Clin Cancer Res 15:876–886
5. Lal S, Clare S, Halas N (2008) Nanoshell-enabled photothermal cancer therapy: impending clinical impact. Accounts Chem Res 41(12):1842–1851
6. Terentyuk G, Maslyakova G, Suleymanova L, Khlebtsov N, Khlebtsov G, Akchurin G, Maksimova I, Tuchin V (2009) Laser-induced tissue hyperthermia mediated by gold nanoparticles: toward cancer phototherapy. J Biomed Opt 14(2):1–9
7. Perrault S, Chan W (2010) In vivo assembly of nanoparticle components to improve targeted cancer imaging. Proc Nat Acad Sci 107(25):11194–11199
8. Chen J, Wiley B, Li ZY, Campbell D, Saeki F, Cang H, Au L, Lee J, Li X, Xie Y (2005) Gold nanocages: engineering their structure for biomedical applications. Adv Mater 17:2255–2261
9. Loo C, Hirsch L, Lee M, Chang E, West J, Halas N, Drezek R (2005) Gold nanoshell bioconjugates for molecular imaging in living cells. Opt Lett 30(9):1012–1014
10. Huang X, El-Sayed I, Qian W, El-Sayed M (2007) Cancer cells assemble and align gold nanorods conjugated to antibodies to produce highly enhanced, sharp, and polarized surface Raman spectra: a potential cancer diagnosis marker. Nano Lett 7:1591–1597
11. El-Sayed I, Huang X, El-Sayed M (2005) Surface plasmon resonance scattering and absorption of anti-EGFR antibody conjugated gold nanoparticles in cancer diagnostics: applications in oral cancer. Nano Lett 5(5):829–834
12. Barton JK, Halas NJ, West JL, Drezek RA (2004) Nanoshells as an optical coherence tomography contrast agent. Proc SPIE 5316:99–106
13. Wang Y, Xie X, Wang X, Ku G, Gill K, O'Neal D, Stoica G, Wang L (2004) Photoacoustic tomography of a nanoshell contrast agent in the in vivo rat brain. Nano Lett 4(9):1689–1692
14. Pitsillides CM, Joe EK, Wei X, Anderson RR, Lin CP (2003) Selective cell targeting with light-absorbing microparticles and nanoparticles. Biophys J 84:4023–4032
15. Sung KB, Liang C, Descour M, Collier T, Follen M, Richards-Kortum R (2002) Fiber-optic confocal reflectance microscope with miniature objective for in vivo imaging of human tissue. IEEE Trans Biomed Eng 49(10):1168–1172
16. Ren X, Chen H, Yang V, Sun D (2014) Iron oxide nanoparticle-based theranostics for cancer imaging and therapy. Front Chem Sci Eng 8(3):253–264
17. Upputuri PK, Huang S, Wang M, Pramanik M (2016) A dual function theranostic agent for near-infrared photoacoustic imaging and photothermal therapy, Proc SPIE 9723, 97230Y San Francisco, California, United States
18. Same S, Aghanejad A, Nakhjavani SA, Barar J, Omidi Y (2016) Radio-labeled theranostics: magnetic and gold nanoparticles. BioImpacts 6(3):169–181
19. Xiong Y, Wang J, Idee J, Corot C (2015) Scientific and industrial challenges of developing nanoparticle-based theranostics and multiple-modality contrast agents for clinical application. Nanoscale 7:16146–16150
20. Shanbhag PP, Iyer V, Shetty T (2017) Gold nanoshells: a ray of hope in cancer diagnosis and treatment. Nucl Med Biol Imag 2(2):1–5
21. Lim EK, Kim T, Paik S, Haam S, Huh YM, Lee K (2015) Nanomaterials for theranostics: recent advances and future challenges. Chem Rev 115(1):327–394
22. Chen W, Zhang S, Yu Y, Zhang H, He Q (2016) Structural-engineering rationales of gold nanoparticles for cancer theranositcs. Adv Mater (Deerfield Beach, Fla) 28(39):8567–8585
23. Guo J, Rahme K, He Y, Li L, Holmes JD, O'Driscoll C (2017) Gold nanoparticles enlighten the future of cancer theranostics. Int J Nanomed 12:6131–6152
24. Pedrosa P, Vinhas R, Fernandes A, Baptista PV (2015) Gold nanotheranostics: proof-of-concept or clinical tool? Nanomaterials 5:1853–1879
25. Vinhas R, Cordeiro M, Carlos FF, Mendo S, Fernandes AR, Figueiredo S, Baptista PV (2015) Gold nanoparticle-based theranostics: disease diagnostics and treatment using a single nanomaterial. Nanobiosensors in Disease Diagnosis 4:11–23
26. Fang W, Wei Y (2016) Upconversion nanoparticle as a theranostic agent for tumor imaging and therapy. J Innov Opt Heal Sci 9(4):1–20

27. Jo SD, Ku SH, Won Y, Kim SH, Kwon IC (2016) Targeted nanotheranostics for future personalized medicine: recent progress in cancer therapy. Theranostics 6(9):1362–1377
28. Sumer B, Gao J (2008) Theranostic nanomedicine for cancer. Nanomedicine 3:137–140
29. Lammers T, Kiessling G, Hennick WE, Storm G (2010) Nanotheranostics and image-guided drug delivery: current concepts and future directions. Mol Pharm 7:1899–1912
30. Janib SM, Moses AS, MacKay JA (2010) Imaging and drug delivery using theranostic nanoparticles. Adv Drug Deliv Rev 62:1052–1063
31. Lammers T, Aime S, Hennink WE, Storm G, Kiessling F (2011) Theranostic nanomedicine. Acc Chem Res 44:1029–1038
32. Lammers T, Rizzo LY, Storm G, Kiessling F (2012) Personalized nanomedicine. Clin Cancer Res 18:4889–4894
33. Zhang XQ, Xu X, Bertrand N, Pridgen E, Swami A, Farokhzad OC (2012) Interactions of nanomaterials and biological systems: implications to personalized nanomedicine. Adv Drug Deliv Rev 64:1363–1384
34. Mura S, Couvreur P (2012) Nanotheranostics for personalized medicine. Adv Drug Deliv Rev 64:1394–1416
35. Vera J, Bayazitoglu Y (2009) Gold nanoshell density variation with laser power for induced hyperthermia. Int J Heat Mass Tran 52:564–573
36. Vera J, Bayazitoglu Y (2009) A note on laser penetration in nanoshell deposited tissue. Int J Heat Mass Tran 52(13/14):3402–3406
37. Xu X, Meade A, Bayazitoglu Y (2013) Feasibility of selctive nanoparticle-assisted photothermal treatment for an embedded liver tumor. Laser Med Sci 28:1159–1168
38. Xu X, Meade A, Bayazitoglu Y (2011) Numerical investigation of nanoparticle-assisted laser-induced interstitial thermotherapy toward tumor and cancer treatment. Laser Med Sci 26:213–222
39. Xu X, Meade A, Bayazitoglu Y (2010) Fluence rate distribution in laser-induced interstitial thermotherapy by meshfree collocation. Int J Heat Mass Tran 53:4017–4022
40. Vera J, Bayazitoglu Y (2009) A note on laser penetration in nanoshell deposited tissue. Int J Heat Mass Tran 52(13/14):3402–3406
41. Eillot AM, Schwartz JS, Wang J, Shetty AM, Biogeny C, O'Neal D, Hazle J, Stafford RJ (2009) Quantitative comparison of delta p1 versus optical diffusion approximations for modeling near-infrared gold nanoshell heating. Med Phys 36(4):1351–1358
42. Lin A, Lewinski N, West J, Halas N, Drezek R (2005) Optically tunable nanoparticle contrast agents for early cancer detection: model-based analysis of gold nanoshells. J Biomed Opt 10(6):064035
43. Feng Y, Rylander MN, Bass J, Oden JT, Diller K (2005) Optimal design of laser surgery for cancer treatment through nanoparticle-mediated hyperthermia therapy. Nano Sci Tech Institute (NSTI) -Nano technology 1:39–42
44. Feng Y, Fuentes D, Hawkins A, Bass J, Rylander MN, Eillot A, Shetty A, Stafford RJ, Oden JT (2009) Nanoshell-mediated laser surgery simulation for prostate cancer treatment. Eng Comput 25:3–13
45. Tjahjono I, Bayazitoglu Y (2008) Near-infrared light heating of a slab by embedded nanoparticles. Int J Heat Mass Tran 51:1505–1515
46. Bayazitoglu Y (2009) Nanoshell assisted cancer thermal therapy: numerical simulations. In: Proceeding the 2nd ASME Micro/Nanoscale Heat Mass Transfer An International Conference Shanghai
47. Bayazitoglu Y, Kheradmand S, Tullius TK (2013) An overview of nanoparticle assisted laser therapy. Int J Heat Mass Tran 67:469–486
48. Bayazitoglu Y (2014) Volumetric laser or solar heating with plasmonic nanoparticles. In: Proceedings of the 15th Int. Heat Transfer Conference, IHTC-15, IHTC15-KN20 Kyoto, Japan, pp 8
49. Lin A (2006) Nanoengineered contrast agents for biophotonics: modeling and experimental measurements of gold nanoshell reflectance, Ph.D dissertation. Rice University, Houston
50. McCarthy JR, Weissleder R (2008) Multifunctional magnetic nanoparticles for targeted imaging and therapy. Adv Drug Delivery Rev 60(11):1241–1251
51. Welch AJ, Gardner C (2002). In: Waynant RW (ed) Optical and thermal response of tissue to laser radiation. Lasers Med, pp 27-45. CRC Press, Boca Raton
52. Jacques SG, Chandrasekar S (1980) Radiative transfer. Oxford University Press, London
53. Ishimaru A (1978) Wave propagation and scattering in random medium. Academic Press, New York
54. Toricelli A, Pifferi A, Taroni P, Giambattistelli E, Cubeddu R (2001) In vivo optical characterization of human tissues from 610-1010 nm by time-resolved reflectance spectroscopy. Phys Med Biol 46:2227–2237
55. Doornbos R, Lang R, Aalders M, Cross F, Sterenborg H (1999) The determination of in vivo human tissue optical properties and absolute chromophore concentrations using spatially resolved steady-state diffuse reflectance spectroscopy. Phys Med Biol 44:967–981
56. Mishra S, Roy H, Misra N (2006) Discrete ordinate method with a new and a simple quadrature scheme. J Quant Spectrosc Rad Tran 101:249–262
57. Fiveland W (1987) Discrete-ordinates solutions of the radiative transport equation for rectangular enclosures. J Heat Tran 109(4):1048–1051
58. Truelove J (1984) Discrete-ordinates solutions of the radiative transport equation. J Heat Tran 106:699–706
59. Chui E, Raithby G, Hughes P (1990) A finite-volume method for predicting a radiant heat transfer in enclosures with participating media. J Heat Tran 112(2):415–423
60. Chai J, Lee H, Patankar S (1994) Finite volume method for radiative heat transfer. J Thermophys Heat Tran 8(3):419–425
61. Henyey L, Greenstein J (1941) Diffuse radiation in the galaxy. Astrophys J 93:70–83
62. Mie G (1908) Beitrage zur Optik truber Medien, speziell kolloidaler metallosungen. Ann Phys 330:377–445
63. Collier T, Lacy A, Richard-Kortum R, Malpica A, Follen M (2002) Near real-time confocal microscopy of amelanotic tissue. Acad Radiol 9(5):504–512
64. Fujimoto JG (2003) Optical coherence tomography for ultrahigh resolution in vivo imaging. Nat Biotechnol 21(11):1361–1367
65. Zeng H, Petek M, Zorman MT, McWilliams A, Palcic B, Lam S (2004) Integrated endoscopy system for simultaneous imaging and spectroscopy for early lung cancer detection. Opt Lett 29(6):587–589
66. Sassaroli E, Li K, Oneill B (2009) Numerical investigation of heating a gold nanoparticle and the surrounding microenvironment by nanosecond laser pulse for nanomedicine applications. Phys Med Biol 54:5541–5560
67. Ratzel AC, Howell JR (1983) Two-dimensional radiation in absorbing-emitting media using the P-N approximation. J Heat Tran 105(2):333–340
68. Matsumura Y, Maede H (1986) A new concept of macromolecular therapies in cancer chemotherapy: mechanism of tumor tropic accumulation of proteins and the antitumor agent SMANCS. Cancer Res 6:6387–6392

69. Maede H, Wu J, Sawa T, Matsumura Y, Hori K (2001) Tumor vascular permeability and the EPR effect in macromolecular therapeutics: a review. J Control Release 65:271–284
70. Maede H, Fange J, Unstuck T, Kitamoto Y (2003) Vascular permeability enhancement in solid tumor: various factors, mechanisms involved and its implications. Int Immunopharmacol 3:319–328
71. Iyer A, Khaled G, Fange J, Maeda H (2006) Exploiting the enhanced permeability and retention effect for tumor targeting. Drug Discov Today 11:812–818
72. Struesson C, Andersson-Engels S, Svanberg S (1995) A numerical model for the temperature increase in surface-applied laser-induced thermo therapy with applications to tumor blood flow estimations, Laser-induced interstitial thermotherapy. SPIE, Bellingham, pp 157–173